Spin Crossover Metal-Organic Frameworks with Inserted Photoactive Guests: On the Quest to Control the Spin State by Photoisomerization

Barbora Brachňaková,[a,b] Ján Moncoľ,[b] Ján Pavlik,[b] Ivan Šalitroš,[b,c,d*] Sébastien Bonhommeau,[e] Francisco Javier Valverde-Muñoz,[f] Lionel Salmon,[a] Gábor Molnár,[a] Lucie Routaboul,[a] Azzedine Bousseksou[a*]

a) LCC, CNRS & Université de Toulouse, 205 route de Narbonne, 31077 Toulouse, France
b) Department of Inorganic Chemistry. Faculty of Chemical and Food Technology. Slovak University of Technology in Bratislava. Bratislava SK-81237, Slovakia.
c) Department of Inorganic Chemistry. Faculty of Science, Palacký University, 17. listopadu 12, 771 46 Olomouc, Czech Republic
d) Central European Institute of Technology, Brno University of Technology, Purkyňova 123, 61200 Brno Czech Republic
e) Univ. Bordeaux, CNRS, Bordeaux INP, ISM, UMR 5255, F-33400 Talence, France
f) Departament de Quimica Inorgànica, Institut de Ciencia Molecular (ICMol), Universitat de Valencia, Valencia, Spain.

* E-mail: ivan.salitros@stuba.sk, azzedine.bousseksou@lcc-toulouse.fr

Abstract. Three Hofmann-like metal-organic frameworks {Fe(bpac)[Pt(CN)$_4$]}·G (bpac=1,2-bis(4-pyridyl)acetylene) were synthesized with photoisomerizable guest molecules (G = *trans*-azobenzene, *trans*-stilbene or *cis*-stilbene) and were characterized by elemental analysis, thermogravimetry and powder X-ray diffraction. The insertion of guest molecules and their conformation were inferred from Raman and FTIR spectra and from single-crystal X-ray diffraction and confronted with computational simulation. The magnetic and photomagnetic behaviors of the framework are significantly altered by the different guest molecules and different conformations. On the other hand, photoisomerization of the guest molecules becomes strongly hindered by the framework.

1. INTRODUCTION

Since their discovery nearly a century ago, spin crossover (SCO) complexes of transition metal ions have been extensively studied due to their unique optical, magnetic, electrical and mechanical properties related to the switching between the low spin (LS) and high spin (HS) electronic configurations.[1] The spin state of these compounds can be modified by various external stimuli such as variation of temperature, pressure, intense magnetic fields, adsorption/desorption of molecules and light irradiation. SCO molecules with the ability to "switch" their properties show appealing application potential in several fields of technology such as information processing devices, sensors and actuators.[2] In this context, light irradiation appears as a fascinating tool for the control of physical properties

of SCO materials. It is well known that photoexcitation can change the population of the LS and HS states *via* ligand-field or charge transfer transitions and subsequent relaxation phenomena.[3] In certain compounds, at very low temperatures, the photoinduced metastable spin state can have a very long lifetime (days-weeks). This famous phenomenon is known in the literature as the Light-Induced Excited Spin State Trapping (LIESST) and was already reported for many ferrous SCO compounds and for a few ferric complexes as well.[4] However, the low temperature that is necessary for the trapping of the photoexcited states can be a drawback for applications. An alternative way to control the spin state of SCO compounds by light is the introduction of photoswitchable ligands capable of reversible transformation between two isomeric forms when exposed to selective wavelengths. Obviously, this photoconversion results in modifications of both the ligand field and the crystal packing and therefore the relative stability of the HS and LS states of the central metal ion will be altered. The Ligand-Driven Light-Induced Spin Crossover (LD-LISC) approach, introduced by Zarembowitch *et al*.,[5] is a fascinating strategy because it can be performed even in ambient conditions. However, only a few compounds exhibit LD-LISC in the solid state and the associated SCO is usually not complete due to the significant steric hindrance for the photoisomerization of the ligands in the solid state.[6]

In analogy with the LD-LISC approach, one could also envision to encapsulate photoisomerizable guest molecules within porous metal-organic frameworks (MOFs) displaying SCO, leading to the novel concept of Guest-Driven Light-Induced Spin Crossover (GD-LISC). Indeed, in the past two decades several SCO-MOFs have been synthesized, the most famous being the Hofmann-type SCO clathrates, pioneered by the team of Real,[7] with compositions {Fe(L)[M(CN)$_4$]} (M = Ni, Pt, Pd; L = pyrazine, 4,4´-bipyridine, 4,4´-azopyridine, 1,2-bis(4-pyridyl)ethylene, 1,2-bis(4-pyridyl)acetylene (bpac) and so forth).[8] The SCO phenomenon in these three-dimensional (3D) porous systems is related to hexa-coordinated iron(II) centers interconnected to each other *via* the pillared organic ligand L in axial direction and *via* the diamagnetic tetracyano-metallate ligand in equatorial directions. A remarkable property of these compounds is that their spin state can be controlled by the nature and quantity of inserted guest molecules (steric effect or ability to create short contact interactions).[9-12] Tuning the SCO properties has been achieved also by the incorporation of 'active' guest molecules displaying chemical reactivity.[12] In the case of photoisomerizable guest molecules, switching from one form to the other is associated with changes of the molecular geometry as well as various physical properties, such as the dielectric permittivity. Therefore, one can assume that photoisomerization should efficiently modulate the phase stability (and associated magnetic properties) of the host system *via* the modification of host-guest interactions.

Several papers have already reported about the introduction of various photochromic molecules into different MOFs and other macrocyclic cage systems and the photoisomerization of the encapsulated molecules have also been demonstrated.[13, 14] The aim of these works was the incorporation of switchable guests within a porous framework and the associated ability to photocontrol their functional properties, such as pore

size,[13a,b] adsorption ability,[13c] optical[13d] or electric[14a] properties and solubility.[14b] However, to our best knowledge, the control of magnetic properties of a MOF by guest isomerization has not yet been reported.

In the present work, we examined the mutual effect of an SCO-MOF and photoisomerizable molecules on their respective switching properties. Specifically, we report on the synthesis and characterization of the Hofmann-like framework $\{Fe(bpac)[Pt(CN)_4]\}\cdot G$ with different photoisomerizable guest molecules (G = *trans*-azobenzene, *trans*-stilbene or *cis*-stilbene). We show that the presence of different guest molecules leads to different magnetic and photomagnetic properties of the host framework, depending on the nature and molecular conformation of the guest molecules. On the other hand, the host network introduces constraint for the photoisomerization of the guest molecules, which mostly extent in their initial configuration.

2. EXPERIMENTAL SECTION

Materials and characterization. Solvents and reagents, including $K_2[Pt(CN)_4]\cdot 3H_2O$, $Fe(BF_4)\cdot 6H_2O$, *trans*-azobenzene, *trans*-stilbene and *cis*-stilbene, were purchased form Sigma-Aldrich and used without further purification. The preparation of the bpac ligand and the host framework $\{Fe(bpac)[Pt(CN)_4]\}\cdot 1.5H_2O\cdot 0.5$bpac was carried out according to Ref. [8e,15]. Elemental analysis for CHN were performed after combustion at 850 °C, using IR detection and gravimetry, by means of a Perkin–Elmer 2400 series II device. Mid-IR spectra of the powders were acquired between 4000 - 600 cm^{-1} in ATR mode using a Perkin Elmer FTIR Frontier spectrometer. UV-VIS spectra of the solutions were acquired between 800 – 200 nm in transmission mode using a Cary 60 spectrophotometer. Irradiation of the stilbene solution was carried out using a 150 W xenon light source and a UV bandpass filter (275-375 nm). Thermogravimetry (TG) measurements were performed in a nitrogen flow at a heating rate of 5 $Kmin^{-1}$ in a Netzsch STA 409 C analyzer. Powder X-ray diffraction (PXRD) patterns of the samples have been collected using a Panalytical MPD XPertPro diffractometer [CuKα1 source, Ge(111) monochromator, X'Celerator detector] within the 2θ range 2-60°.

Synthesis of $\{Fe(bpac)[Pt(CN)_4]\}\cdot$*trans*-azobenzene (**1** and **1b**). $K_2[Pt(CN)_4]\cdot 3H_2O$ (100 mg, 0.23 mmol, 1.0 eq) and equivalent amount of *trans*-azobenzene (42 mg, 0.23 mmol, 1.0 eq) were dissolved in 30 cm^3 water-methanol mixture (1:1). Dropwise addition of water-methanol mixture (1:1, 30 cm^3) with dissolved bpac (42 mg, 0.23 mmol, 1.0 eq) and $Fe(BF_4)_2\cdot 6H_2O$ (78 mg, 0.23 mmol, 1.0 eq) led to the formation of an orange colored solution that was stirred under Ar atmosphere for 2 hours at room temperature (RT). The experimental apparatus was not protected against daylight. The precipitated orange powder **1** was filtered off and washed with water (5 cm^3), methanol (5 cm^3) and diethyl ether (5 cm^3). The same synthetic procedure was repeated to obtain compound **1b**. Single-crystals suitable for X-ray diffraction analysis were obtained by slow crystallization in H-tube.[8e] $Fe(NH_4)_2(SO_4)_2.6H_2O$ (30.5 mg, 0.07 mmol, 1.0 eq) and bpac (14 mg, 0.07 mmol, 1.0 eq) were dissolved in 4 cm^3 water:ethanol mixture (1:1) and poured into one side of the H-tube and the other side was filled by $K_2[Pt(CN)_4]\cdot 3H_2O$ (33.3

mg, 0.07 mmol, 1.0 eq) dissolved in 2 cm^3 water. The system was finally filled by a water:ethanol (1:1) solution of azobenzene (14 mg, 0.07 mmol, 1.0 eq). After 10 weeks small, thin, square-shaped, red crystals were obtained. Elemental analysis for {Fe(bpac)[Pt(CN)$_4$]}·*trans*-azobenzene ($C_{28}H_{20}FeN_8OPt$, M_w = 717.43 g.mol^{-1}), found % (expected %) for **1**: C 45.79 (46.88), N 15.57 (15.62), H 1.84 (2.53); and for **1b**: C 45.80 (46.88), N 15.52 (15.62), H 1.96 (2.53). FTIR ($\tilde{\nu}_{max}$/cm^{-1}) for **1**: 2165 (s, CN), 1609, 1548 (m, C-C_{ar} and C_{ar}-N), 1484, 1453, 1421 (m, C_{ar}-N and/or C-C_{ar}); and for **1b**: 2166 (s, CN), 1609, 1547 (m, C-C_{ar} and C_{ar}-N), 1484, 1454, 1421 (m, C_{ar}-N and/or C-C_{ar}).

Synthesis of {Fe(bpac)[Pt(CN)$_4$]}·H$_2$O·*trans*-stilbene (**2** and **2b**). $K_2[Pt(CN)_4]\cdot 3H_2O$ (100 mg, 0.23 mmol, 1.0 eq) and *trans*-stilbene (45.6 mg, 0.25 mmol, 1.1 eq) were dissolved in a water-ethanol mixture (1:2, 40 cm^3). The solution was stirred under Ar atmosphere for 30 minutes at RT and a water-ethanol mixture (1:1, 20 cm^3) with dissolved $Fe(BF_4)_2\cdot 6H_2O$ (78.0 mg, 0.23 mmol, 1.0 eq) and bpac (42 mg, 0.23 mmol, 1.0 eq) was added dropwise. The experimental apparatus was not protected against daylight. After 2 hours of stirring, the yellow solid product **2** was filtered off and washed with water (5 cm^3), methanol (5 cm^3) and diethyl ether (5 cm^3). The same synthetic procedure was repeated to obtain compound **2b**. Elemental analysis for {Fe(bpac)[Pt(CN)$_4$]}·H$_2$O·*trans*-stilbene ($C_{30}H_{22}FeN_6OPt$, M_w = 733.46 g.mol^{-1}), found % (expected %) for **2**: C 49.94 (49.13), N 10.88 (11.46), H 2.17 (3.02); and for **2b**: C 50.18 (49.13), N 11.07 (11.46), H 2.28 (3.02). FTIR ($\tilde{\nu}_{max}$/cm^{-1}) for **2**: 2163 (s, CN), 1609, 1546 (m, C-C_{ar} and C_{ar}-N), 1497, 1452, 1420 (m, C_{ar}-N and/or C-C_{ar}); and for **2b**: 2164 (s, CN), 1609, 1547 (m, C-C_{ar} and C_{ar}-N), 1497, 1453, 1421 (m, C_{ar}-N and/or C-C_{ar}).

Synthesis of {Fe(bpac)[Pt(CN)$_4$]}·2.3H$_2$O·0.6*cis*-stilbene (3 and 3b). $K_2[Pt(CN)_4]\cdot 3H_2O$ (100 mg, 0.23 mmol, 1.0 eq) and cis-stilbene (0.9 cm^3, 0.50 mmol, 2.2 eq) were dissolved in a water-ethanol mixture (1:2, 30 cm^3) and stirred under Ar atmosphere over 30 minutes at RT. Then, a water-ethanol mixture (1:2, 30 cm^3) with dissolved $Fe(BF_4)_2\cdot 6H_2O$ (78.0 mg, 0.23 mmol, 1.0 eq) and bpac (42 mg, 0.23 mmol, 1.0 eq) was added dropwise. The experimental apparatus was not protected against the daylight. The suspension was stirred for 2 hours and the yellow solid product **3** was then filtered off and washed with ethanol (10 cm^3) and diethyl ether (10 cm^3). The same synthetic procedure was repeated to obtain compound **3b**. Elemental analysis for {Fe(bpac)[Pt(CN)$_4$]}·2.3H$_2$O·0.6*cis*-stilbene ($C_{24.4}H_{19.8}N_6O_{2.3}FePt$, M_w = 684.75 g.mol^{-1}), found % (expected %) for **3**: C 42.02 (42.79), N 9.06 (12.27), H 1.69 (2.91); and for **3b**: C 43.80 (42.79), N 10.04 (12.27), H 1.85 (2.91). FTIR ($\tilde{\nu}_{max}$/cm^{-1}) for **3**: 2165 (s, CN), 1609, 1546 (m, C-C_{ar} and C_{ar}-N), 1495, 1448, 1443, 1421 (m, C_{ar}-N and/or C-C_{ar}); and for **3b**: 2165 (s, CN), 1609, 1547 (m, C-C_{ar} and C_{ar}-N), 1494, 1949, 1443, 1421 (m, C_{ar}-N and/or C_{ar}-C_{ar}).

Post-synthetic guest insertion experiments. Compounds **1c-3c** with *trans*-azobenzene, *trans*-stilbene and *cis*-stilbene guests, respectively, have been synthesized by the inclusion of the guest molecules into the cavities of the previously synthesized host framework {Fe(bpac)[Pt(CN)$_4$]}1.5H$_2$O·0.5bpac in 1:1 ratio in an ethanol-water mixture (1:1, 20 cm^3). The mixture was stirred under Ar atmosphere at RT for 24 hours, filtered off and dried by 10 cm^3 diethyl ether.

Single-crystal X-ray diffraction analysis. Data collection and cell refinement of **1** at 100 and 180 K were made using a Stoe StadiVari diffractometer. The diffractometer was equipped with an HPAD detector (Pilatus3R 300K) and a microfocused X-ray source (Xenocs Genix3D Cu HF). The programs ShelXT, ShelXL (ver. 2018/3), OLEX2 and MERCURY have been used for structure determination, refinement, finalization and drawing.[16]

Computational details. All calculations were performed using the program ORCA 4.2.0.[17a-b] The effect of encapsulation of azobenzene and stilbene isomers was studied by the QM/MM strategy as follows: an electrically neutral cut off from the low-spin and high-spin MOF cavity was defined (**Fig. SI-8**), which was considered a rigid body and treated by molecular mechanics (MM), whereas the encapsulated molecule was subject of geometrical optimization, vibrational and Raman analysis employing quantum mechanics (QM). The geometry of cavities was fixed as resulted from X-ray analysis except of positions of hydrogen atoms, which were optimized by the method PBEh-3c.[17c] Precise orientation of molecule of *trans*-azobenzene was known from the X-ray analysis, all other molecules were manually put in similar position and optimized. The additive coupling and electrostatic embedding schemes were used. The charges at MOF atoms were obtained by the CHELPG method[17d] after a successfully converged DFT calculation. This was performed with the GGA functional PBE[17e] and the def2-SVP basis[17f] for all atoms, except of Pt for which the effective core potential def2-ECP[17g] was used. The Coulomb term was treated by the resolution of identity approach (RI-J)[17h] with the Coulomb fitting basis set def2/J.[17i] Increased integration grid was used (grid7 in ORCA convention). Since all metallic centres are structurally equivalent, in ideal case the values of CHELPG charges should be equal for all Pt atoms and Fe atoms. Obviously, this will not be obeyed for a finite-size cavity. Comparison of calculated values of CHELPG charges shows that smaller error is introduced in the case of LS cavity where all values are closer to each other (**Fig. SI-9**). The geometry of the embedded molecules was optimized using the same GGA functional PBE and a higher-quality basis def2-TZVP[18f] with the same approximation to the Coulomb term as mentioned above. No negative vibration frequencies were found. The Raman spectra were calculated within a development version of ORCA 4.2.

Raman spectroscopy. Raman measurements were carried out in backscattering geometry using commercial, confocal Raman microspectrometers (Horiba Scientific), including a Labram HR Evolution spectrometer (focal length f=800 mm, grooves density G=2400 mm^{-1}, objective magnification m=5x, laser excitation wavelength λ=355 nm and power P=0.9 mW), an XploRA spectrometer (f=250 mm, G=1200 mm^{-1} or 2400 mm^{-1}, m=100x or 50 x, λ=785 or 532 nm, P=0.4 or 1 mW, respectively) and a Labram HR800 spectrometer (f=800 mm, G=600 mm^{-1}, m=50x, λ=532 nm, P=1 mW). The frequency calibration was systematically performed by checking the 520 cm^{-1} Raman mode of a reference Si sample. Standard deviations on wavenumbers were lower than 1 cm^{-1}. The sample temperature was set using a Linkam THMS600 liquid-nitrogen-cooled cryostage. Owing to the microcrystalline nature of the analyzed samples the polarization dependence of the spectra was not investigated.

Magnetic and photomagnetic experiments. Magnetic property measurements were performed using a MPMS-XL7 and a PPMS VersaLab instrument (Quantum Design). For magnetic susceptibility measurements in the dark, the temperature dependent magnetization was recorded under an external magnetic field of 0.1 T at sweeping rates of ±1 K min^{-1}. The data were corrected for the diamagnetic contributions. Photomagnetic measurements were performed using a diode-pumped solid-state laser Kvant (λ = 637 nm, 300 mW) coupled through an optical fiber to the cavity of the magnetometer. The power on the sample was adjusted to 10 $mWcm^{-2}$. For the photomagnetic experiments, a small amount of sample (≈1 mg) was diluted in melted eicosane, introduced into the measuring plastic straw and solidified. The weight of the samples was obtained by comparison with the thermal χT vs. T curve of a more accurately weighed sample of the same compound. After cooling to 5 K, the sample was irradiated and the change in magnetization was followed. After reaching the saturation point, the light was switched off, the temperature was increased at a rate of 0.3 K min^{-1} and the magnetization was measured at 1 K intervals. The so-called T(LIESST) value[18] was determined as the temperature for which the $\partial(\chi T)/\partial T$ vs. T derivative function reaches a minimum.

3. RESULTS AND DISCUSSION

3.1. Synthesis of the host-guest systems

For the present work we have chosen the {Fe(bpac)[$Pt(CN)_4$]} clathrate network,[8e,15] which exhibits thermal SCO near room temperature with hysteresis. The large pore size in this system (ca. 300 $Å^3$ in the denser LS state) allows relatively bulky guest molecules to be hosted. Notably, photoisomerizable molecules, such as azobenzene and stilbene, whose size roughly matches the size of the cavities, can be incorporated *a priori*. This can provide the scope for the light-induced modulation of the spin state of the host framework due to the *trans-cis* photoisomerization of the guest molecules.

Azobenzene and stilbene (and their derivatives) are well-known photochromic molecules with various applications.[19-21] These molecules are able to undergo reversible interconversion between the *trans* (E) and *cis* (Z) isomers induced by light or by thermal activation. The switching from the *trans* to the *cis* form can be induced by ultraviolet light in both compounds, whereas the reverse conversion is achieved by visible (resp. UV) light for azobenzene (resp. stilbene) or by heating. It is important to note that the isomerization of azobenzene (resp. stilbene) is associated with the variation of planarity of guest molecules as well as with the change in their lengths by ca. 2.9 Å (resp. 2.3 Å) and volume by ca. 3.7 $Å^3$ (resp. 1.0 $Å^3$). The guest molecules in the *trans* conformation may create a sandwiched or slipped stacking with the pillared bpac ligands and build intermolecular interactions.[8e,12] Obviously, when going from the *trans* to the *cis* configuration, the loss of planarity leads to altered interactions with the host framework.[12c]

We tested different approaches, which were reported in the literature[15] for the synthesis of {Fe(bpac)[$Pt(CN)_4$]} with guest molecules. It turned out that the building of the host network in the presence of guest molecules (compounds **1-3** and **1b-3b**) seems to be the most favorable strategy to maximize the inclusion of photochromic guests and

minimize the quantity of uncoordinated bpac molecules within the cavities of the host. Although the presence of *trans*-azobenzene (**1c**), *trans*-stilbene (**2c**) and *cis*-stilbene (**3c**) is also visible in the vibrational spectra following post-synthetic inclusion of guests, the fingerprint of uncoordinated bpac ligand in **1c-3c** is also detected around 1599 cm^{-1} and 997 cm^{-1} in the FTIR and Raman spectra, respectively (see **Fig. SI-1** in the Supporting Information, SI). For this reason, we focused our attention mostly on the investigation of compounds **1**-**3** and **1b**-**3b**. The quantity of included guests in the different clathrates was estimated by combination of elemental analysis and thermogravimetric measurements (see **Fig. SI-2**) which resulted in molecular formula $\{Fe(bpac)[Pt(CN)_4]\}\cdot$*trans*-azobenzene (**1** and **1b**), $\{Fe(bpac)[Pt(CN)_4]\}\cdot H_2O\cdot$*trans*-stilbene (**2** and **2b**) and $\{Fe(bpac)[Pt(CN)_4]\}\cdot 2.3H_2O\cdot 0.6$cis-stilbene (**3** and **3b**). The TG profile of the host network is comparable with the literature[8e] and indicates the stability of each host-guest system up to 370 K. The azobenzene clathrate exhibits a single abrupt mass loss above 500 K attributed to the liberation of *trans*-azobenzene molecules, whereas the stilbene clathrates exhibit mass loss in two steps. The first step is assigned to release of water molecules and takes place above 370 K, while the second step above 450 K is related to the release of bpac molecules.

3.2. Identification of the guest molecules in the host framework

Different thermal stability of compounds **1-3**, revealed by the TG measurements, is a first indication of the successful introduction of the three different guest molecules in the cavities of the frameworks. Infrared absorption and Raman scattering spectroscopies were used to confirm their presence and assess their configuration. The infrared absorption peaks of compounds **1-3** have been confronted with the FTIR spectra of the host clathrate and pure guest molecules (see **Fig. 1** and **Tab. SI-3**). The FTIR spectrum of the host compound $\{Fe(bpac)[Pt(CN)_4]\}\cdot 1.5H_2O\cdot 0.5$bpac contains an intense peak at 2170 cm^{-1} characteristic for the cyanide group. The spectral range between 1800 and 600 cm^{-1} is characteristic of the bpac ligand, whereas in the low frequency range (< 600 cm^{-1}) one would expect mostly vibrations associated with the 2D $\{Fe[Pt(CN)_4]\}$ sheets.[22] The spectrum of the host system involves two peaks at 1612 cm^{-1} and 1599 cm^{-1} that can be assigned to coordinated and uncoordinated bpac molecules, respectively. This indicates that the host framework contains uncoordinated guest bpac molecules. A small shift to 1609 cm^{-1} of the coordinated bpac is observed in compounds **1-3** and no signal of uncoordinated ligands is present. The vanishing of the 995 cm^{-1} peak in compounds **1-3** further supports the absence of clathrated bpac molecules. We can also note a small shift of the 1018 cm^{-1} IR peak (host system) to 1015 cm^{-1} (compound **1**) and 1016 cm^{-1} (compounds **2** and **3**), attributed to the breathing of coordinated bpac molecules, which indicates different interactions between the pillared ligand and the various guest molecules.

In the spectrum of **1** two peaks at 1484 and 1453 cm^{-1} can be assigned to the in-plane bending of phenyl groups with *trans* configuration of azobenzene.[23] A peak at 927 cm^{-1} corresponds to C-C and C-C-N aromatic ring deformation vibrations, whereas the most intense peaks centered at 776 and 691 cm^{-1} are assigned to the out-of-plane C-C and

C-H vibrational modes of azobenzene aromatic rings.[24] On the other hand, IR spectra of compounds **2** and **3** are comparable, with only a few peaks allowing the *trans* and *cis* configurations of stilbene to be distinguished from each other. Peaks at 1497 (resp. 1495) and 1452 (resp. 1448) cm^{-1} for compound **2** (resp. **3**) are assigned to the in-plane C-H bending of aromatic ring of stilbene molecules. Below 1000 cm^{-1}, the IR peak at 963 cm^{-1} indicates the presence of *trans*-stilbene in compound **2**. Based on previous calculations,[25] this peak can be assigned to the C-H bending modes of the benzene ring. In contrast, *cis*-stilbene shows a few specific features in compound **3**, namely a peak at 922 cm^{-1} attributed to an out-of-plane C-H bending of the aromatic ring, and two others at 777 and 751 cm^{-1} (also present in pure *cis*-stilbene) assigned to the aromatic ring deformation or torsional modes.[25,26] These differences support the selective insertion of *trans*- and *cis*-stilbene into the cavities without structural interconversion during the synthesis of MOFs.

This conclusion is also supported by UV-VIS absorption spectroscopy that was carried out to verify if isomerization of stilbene occurs under the reaction conditions used for the synthesis of **2** and **3**. The water-ethanol solutions of pure *trans*- or *cis*-stilbene were stirred over 2 hours and the UV-VIS absorption spectra were collected (see **Fig. SI-4**). These spectra show that absorption bands of *trans*-stilbene at 295 and 308 nm and *cis*-stilbene at 277 nm remain unchanged over the whole experiment, thus indicating an excellent stability of the compounds in our synthesis conditions.

To gain further insight on the insertion of the guest molecules, Raman spectra of compounds **1-3** were collected and compared with spectra of pure guest molecules (see **Fig. SI-5**) and the host compound $\{Fe(bpac)[Pt(CN)_4]\}\cdot 1.5H_2O\cdot 0.5bpac$ (see **Tab. SI-6**). Raman spectra of **1-3** excited at 532 nm display features similar to those observed in $\{Fe(bpac)[Pt(CN)_4]\}$.[22,27] The signature of guest molecules is visible in the 1000-1600 cm^{-1} spectral range. The most intense Raman peaks of *trans*-azobenzene in **1** are centered at 1145, 1438, 1473 and 1492 cm^{-1} and can be assigned to vibrational modes involving C-N, N=N, N=N + C-N and C=C + N=N stretches, respectively, as well as CCH, CNN and NCC in-plane bends.[28] In addition, several weak peaks at 1186, 1316 cm^{-1} and a shoulder at 1594 cm^{-1} are discernable. Raman spectra of **2** and **3** contain several intense peaks that can be assigned to stilbene guest molecules on the basis of literature data.[25,29,30] An intense Raman peak, corresponding to vinyl C=C stretching vibrations, appears for both isomers at ca. 1630 cm^{-1} (though less intense and redshifted in the *cis* isomer). This peak is a sensitive indicator of electronic delocalization in the molecule. In the pure *cis* and *trans*-stilbene samples, this mode is observed at 1629 and 1637 cm^{-1}, respectively. In the host framework this mode is redshifted to ca. 1632 cm^{-1} for the *trans* conformer, whereas it remains nearly unchanged for the clathrated *cis* isomer.

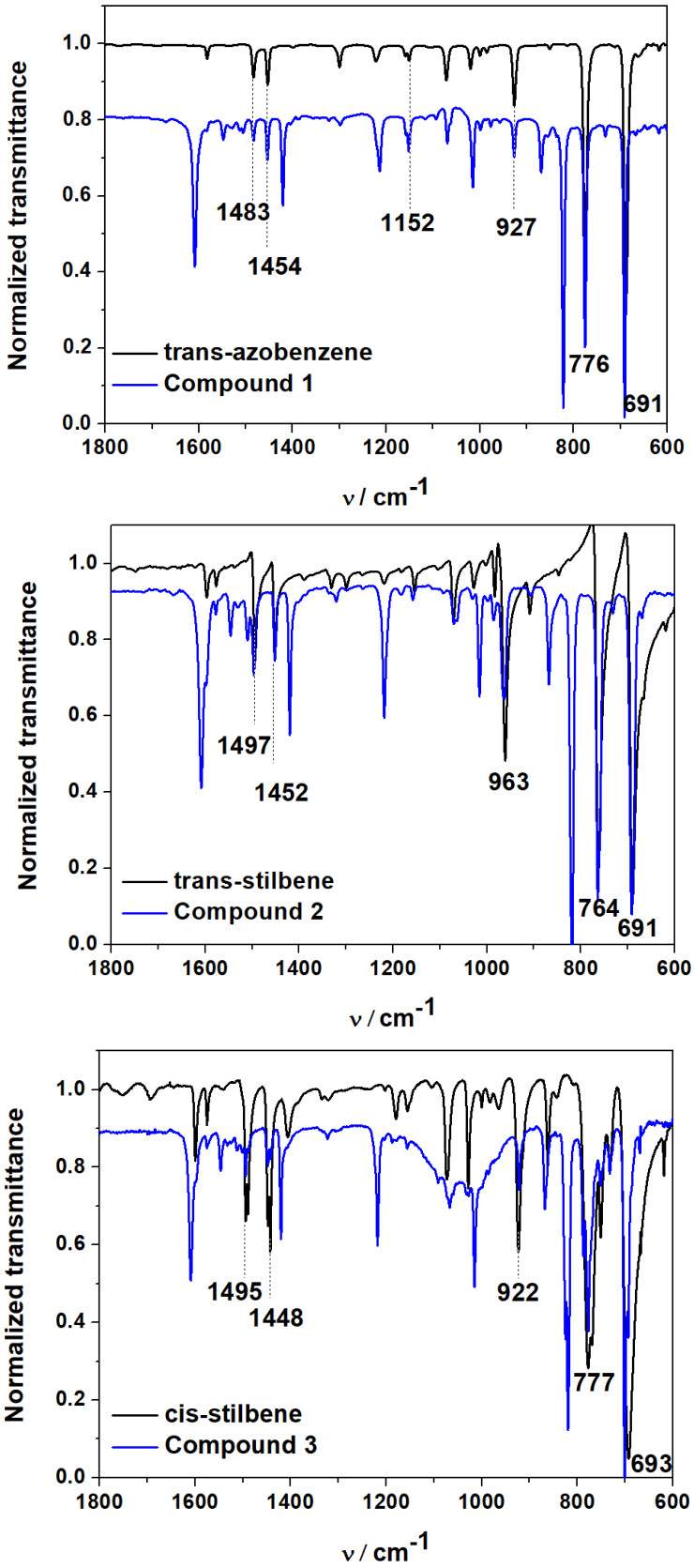

Figure 1. Room temperature FTIR spectral fingerprints of guest molecules in compounds **1**-**3**.

This is a compelling indication of intermolecular interactions between the bpac ligands and *trans*-stilbene guest molecules, resulting in a weaker C=C bond due to its coupling to the aromatic rings by electronic delocalization. Two other intense peaks can be discerned at ca. 1595 cm^{-1} (assigned to C=C ring stretching modes) and at 1191 cm^{-1} (assigned to C-H bending modes of aromatic rings). [25a,30] Other weak intensity peaks originating from stilbene were found between 1300 and 1500 cm^{-1} corresponding to C-H bending and C=C stretching vibrations of phenyl rings.[30] One can differentiate the two isomers using a weak intensity peak at ca. 960 cm^{-1} (identified as in-phase ethylenic C-H out-of-plane wagging vibration)[30,31] which is only present in the *cis* configuration, due to its nonplanar structure.

In order to support the peak assignments, computer simulation of the encapsulation of photoisomerizable molecules was performed. The quantum mechanics/molecular mechanics method (QM/MM) was used. In this hybrid approach, a part of the studied system is selected, which is responsible for electronic properties and it is treated by the laws of quantum mechanics (QM). Rest of the system is a subject of classical Newtonian mechanics (molecular mechanics, MM). The MM part was defined here by cutoff from respective HS or LS host lattice (see **Fig. SI-8**) and its geometry was fixed rigid as it resulted from the X-ray study (*vide infra*). The QM part was formed by one of photoisomerizable guest molecules. The effect of host upon the geometry and vibrational behavior of guest molecules was mediated by electrostatic interactions (for more information see Computational details and ESI). The computed FTIR and Raman spectra of free and encapsulated guest molecules are shown in **Fig. SI-7** and **Tab. SI-10**, **SI-11**. The overall agreement between the computed and experimental spectra is satisfactory, allowing us to extend and confirm the spectral assignments.

The presence of guest molecules in compound **1** was also confirmed by single crystal X-ray diffraction analysis. The crystal structure was resolved at 100 K and 180 K in order to characterize the LS and HS states of the compound (*vide infra*). Selected crystallographic information are listed in **Tab. SI-12**. The insertion of *trans*-azobenzene changed the crystal symmetry compared to previously reported {Fe(bpac)[$M(CN)_4$]}·guest structures with uncoordinated bpac, toluene or 2,4,6-trichlorophenol molecules, all crystallizing in the tetragonal P4/mmm space group.[8e] In the 100 - 180 K temperature range, compound **1** crystallizes in the triclinic P-1 space group. The thermal evolution of unit cell parameters (see **Fig. SI-13**) revealed a first-order phase transition accompanying the SCO with hysteresis and no change in the space group. This phase transition occurs above 165 K on the heating branch of the hysteresis loop and below 140 K on the cooling branch (see **Fig. SI-13**). Remarkably, while the *a* and *b* lattice constants increase with temperature ($\Delta a \approx +0.08$ Å, $\Delta b \approx +0.24$ Å), the *c* lattice constant notably decreases ($\Delta c \approx -0.36$ Å) upon the SCO, resulting in a lattice volume expansion of 3 %, which is markedly smaller when compared to other {Fe(bpac)[$M(CN)_4$]}·guest structures. In both, the low- and high-temperature structures of **1**, the unit cell involves one monomeric unit {Fe(bpac)[$Pt(CN)_4$]}·*trans*-azobenzene and the asymmetric unit contains half the iron(II) central atom, half the $[Pt(CN)_4]^{2-}$ anion, and half bpac and *trans*-azobenzene molecules. The crystal structure of **1** consists of 2D inorganic {Fe[$Pt(CN)_4$]}

sub-layers which are interconnected through bpac bridging ligands (**Fig. 2**). The voids contain *trans*-azobenzene molecules situated between two bpac ligands in face-to-face fashion, albeit turned with respect to the direction of bpac pillars by ca. 34° at 100 K and ca. 30° at 180 K (see **Fig. SI-14**). Since the closest distances between two bpac and *trans*-azobenzene exceed 3.5 Å (see **Fig. SI-14**), guest molecules should form weak non-covalent contacts with neighbor bpac ligands from both sides. The closest intermolecular distance between two guest molecules is measured between the *meta* carbon atom of phenyl ring (C13) and the nitrogen atom (N4) of the azo bond (3.8137(1) Å at 100 K and 3.8787(2) Å at 180 K). The Fe-N distances of the low temperature structure are 1.926(6) Å (Fe-N1, Fe-N2) and 2.008(5) Å (Fe-N3), which is consistent with LS Fe(II) metal centers (see **Fig. SI-14**). On the other hand, those bonds are notably longer 2.137(8) Å (Fe-N1), 2.153(8) Å (Fe-N2) and 2.217(9) Å (Fe-N3) at 180 K indicating HS Fe(II) centers. Furthermore, the thermal SCO affected several features of the supramolecular network. For instance, the C2-N2-Fe1 angle diminishes from 165.185(3)° (100 K) to 159.255(4)° (180 K) due to the lengthening of the Fe-N2 bonds upon the SCO. The most apparent SCO-induced change of the supramolecular structure is observed on the 2D sub-layers {Fe[Pt(CN)$_4$] }, where the angle N1-C-Pt is 177.453(3)° at 100 K, but falls to 159.255(4)° at 180 K. The distances between the nearest Fe(II) atoms are 6.8681(2) Å (along the *a*-axis), 7.3161(2) Å (along the *b*-axis) and 13.6256(6) Å (along the *c*-axis) at 100 K and 6.9483(3) Å (along *a* axis), 7.5509(2) Å (along *b* axis) and 14.0040(6) Å (along *c* axis) at 180 K.

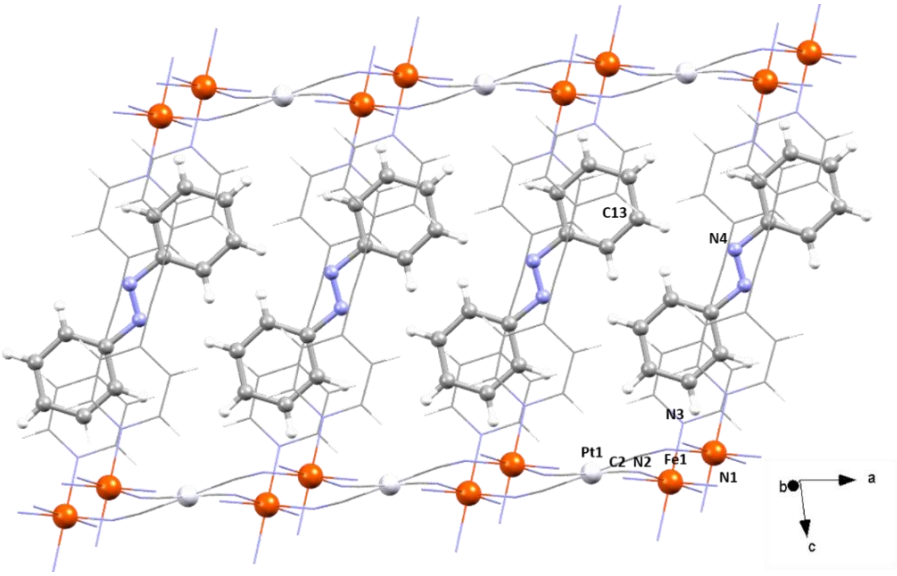

Figure 2. Supramolecular structure of compound **1**. (Fe-orange, Pt-white, C-grey, N-blue, H-white.)

3.3. Spin crossover properties of the host-guest compounds

Some of us have previously reported on the effect of various guest molecules on the SCO properties of {Fe(bpac)[Pt(CN)$_4$]}. The empty host framework exhibits incomplete SCO situated just below room temperature,[8e,15] whereas the presence of uncoordinated bpac molecules (or other small aromatic molecules) in the cavities results in more complete near room temperature SCO associated with thermal hysteresis (see **Fig. SI-15**), whose

width and position are strongly dependent of the number and the nature of guest molecules.[8e,12e,32] It was shown that both electronic and steric interactions contribute to the SCO properties of the host-guest systems.[33] Hence, one would naturally expect that the different photoisomerizable molecules used in the present study give rise to different SCO behaviours.

The temperature dependence (100-300 K) of the Raman spectra (532 nm excitation) was first used for the spectroscopic confirmation of the SCO properties of the samples. Indeed, the spectra show several changes when the molecules undergo SCO (**Fig. 3**). At 293 K, the Raman peak at 1017 cm^{-1} for **1** (1014 cm^{-1} for **2** or **3**) can be assigned to the ring breathing of the coordinated bpac ligand. At 113 K, the Fe(II) centers are partially converted to the LS state and a new peak at 1027 cm^{-1} appears for **1** (1026 cm^{-1} for **2** and **3**). The temperature dependence of the relative intensity of the 1017 cm^{-1} and 1027 cm^{-1} peaks allows for the identification of the temperature range for which the SCO occurs. The observed transition temperatures ($T_{1/2}$) are ca. 135 K for **1**, 173 K for **2** and 162 K for **3** (see **Fig. SI-16**). In other words, the introduction of *trans*-azobenzene, *cis*-stilbene or *trans*-stilbene within the {Fe(bpac)[$Pt(CN)_4$]} host matrix leads to a marked lowering (well below room temperature) of the temperature at which the SCO event occurs.

For a more quantitative investigation of the SCO properties, we acquired magnetic susceptibility data in two consecutive cooling-heating cycles for each sample (**Fig. 4** and **Fig. SI-17**). Compound **1** exhibits a virtually complete, abrupt SCO with hysteresis. At 300 K, the χT product reaches a value of 3.81 cm^3Kmol^{-1}, which remains constant down to 150 K. The subsequent drop of χT around $T_{1/2}\downarrow$ = 137 K indicates the SCO phenomenon. At 50 K, the χT product reaches a value of 0.35 cm^3Kmol^{-1}. Upon heating, the SCO occurs around $T_{1/2}\uparrow$ = 148 K, denoting a hysteresis width of ca. 11 K. (N.B. The different transition temperatures observed in XRD experiments must arise most likely due to the different guest content of single crystal and powder samples.) Red-light irradiation (637 nm) of the LS sample **1** was performed at 5 K and revealed an increase of the χT value with time up to 0.86 cm^3Kmol^{-1} (**Fig. 4**, red triangles). This is the sign that the compound exhibits LIESST effect. (N.B. This LS→HS photoswitching should not be confused with the photoisomerization of the guest, which is not possible in the red wavelength range!) Subsequent heating in the dark revealed a further increase of χT, which can be attributed to the zero-field splitting in HS Fe(II).[12,32] The maximal χT value of 1.52 cm^3Kmol^{-1} was reached at 27 K denoting that ca. 1/3 of the Fe centers have been photo-converted to the HS state (**Fig. 4**, white squares). Upon further heating, the thermally-induced relaxation from the photo-excited HS state back to the LS ground state takes place with a 56 K T(LIESST) temperature.

The introduction of *trans*- and *cis*-stilbene molecules into the cavities of {Fe(bpac)[$Pt(CN)_4$]} leads also to dramatic changes in the SCO properties. Compounds **2** and **3** remain predominantly in the HS state, on cooling down to 224 K (χT = 3.36 cm^3Kmol^{-1}) and 205 K (χT = 2.84 cm^3Kmol^{-1}), respectively.

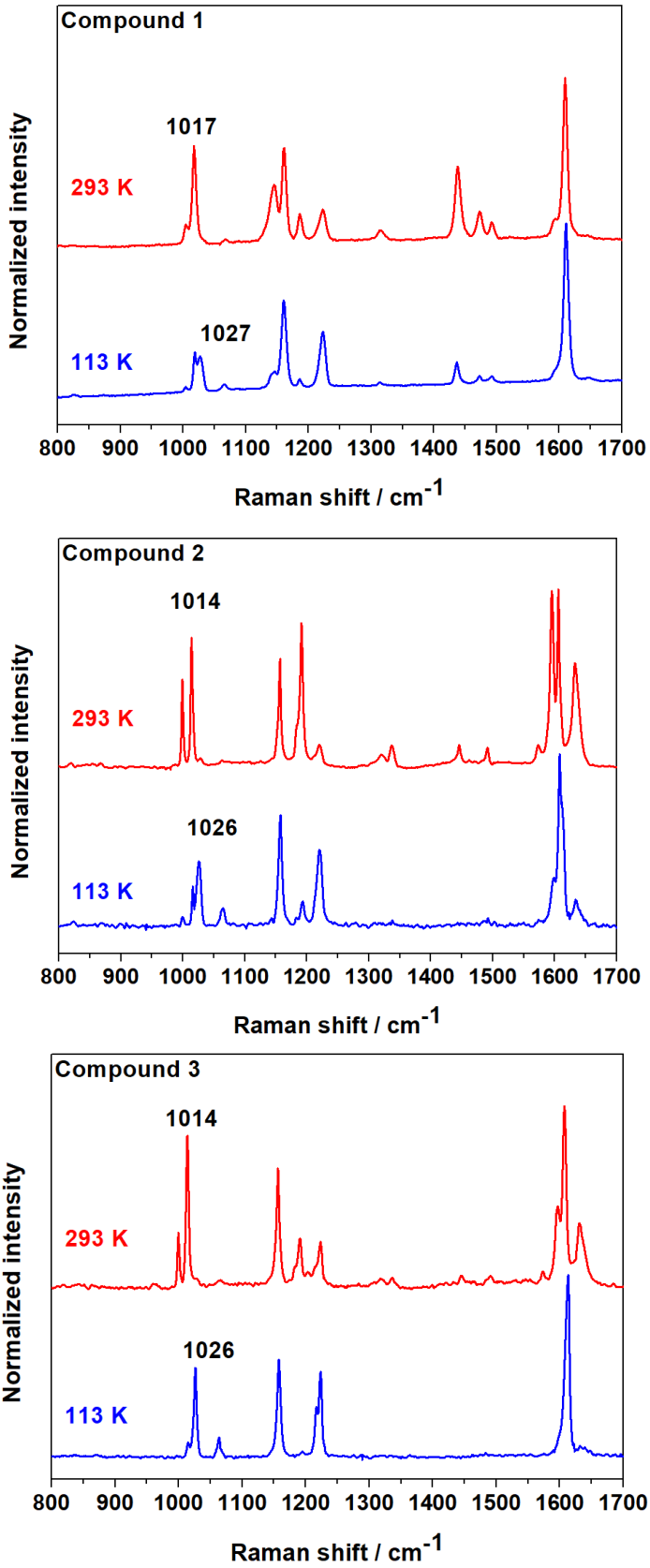

Figure 3. Raman spectra (532 nm excitation) of compounds **1-3** recorded at 293 K and 113 K.

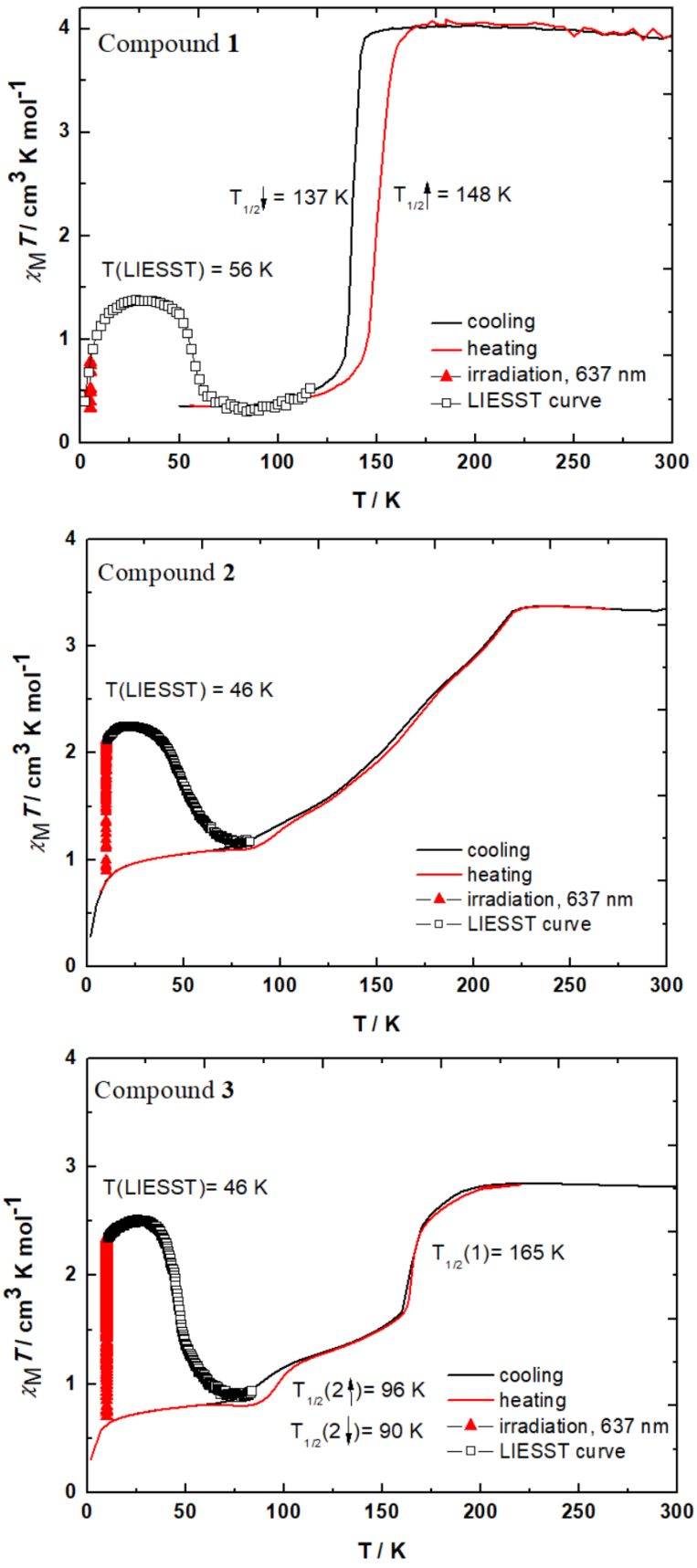

Figure 4. Magnetic properties (χT product) as a function of T for compounds **1**-**3** on cooling and heating (solid lines). Photoexcitation by red light at 5 K or at 10 K (red triangles) and subsequent heating in the dark (white squares) is also shown.

Further cooling revealed a stepwise SCO in both systems. Since the two steps of the SCO in **2** are gradual and not well separated, it is difficult to determine unambiguously the $T_{1/2}$ values for each step (**Fig. 4**). The low-temperature plateau reaches ~1.0 $cm^3mol^{-1}K$ corresponding to ca. 30 % of molecules in the residual, 'frozen' HS state. The tiny hysteresis loop in the low temperature step of the transition has therefore likely a kinetic origin associated with slow relaxation (on the timescale of the magnetic measurements). Compound **3** exhibits also two-step SCO behavior between ca. 205 - 60 K (**Fig. 4**). The first transition is centered at $T_{1/2}(1)$ = 165 K and associated with an abrupt decrease of χT down to 1.52 cm^3Kmol^{-1}, which nearly corresponds to the χT value expected for a 50 % HS→LS conversion of the Fe(II) centers. The second and more gradual step is accompanied by kinetic effects and involves about 30 % of the Fe(II) centers. The χT value of the low-temperature plateau (~0.74 cm^3Kmol^{-1}) indicates that ca. 25 % of the Fe(II) centers remain trapped in the HS state. Red-light irradiation at 10 K led to an increase of the magnetic moment, denoting LIESST activity both in **2** and **3**. The photoconversion is almost complete in **3** (90 % of HS centers at 27 K) and remains largely incomplete in **2** (ca. 65 % of HS centers at 22 K), whereas the T(LIESST) temperatures are virtually the same for both compounds (ca. 46 K).

In line with previous results,[12,15] the strong decrease of the SCO temperature (i.e. the stabilization of the HS phase) most probably indicates that steric effects dominate the spin-transition behavior of the host-guest systems **1-3**. It is tempting to associate the different SCO features in compounds **2** and **3** with the different conformation of stilbene guests (*trans* vs. *cis*). However, the differences could be also attributed (at least partly) to the different amount of guest molecules in the two samples.[8e,12c,15] In order to better apprehend this issue, we prepared a second series of samples (**1b**-**3b**) under the same synthesis conditions, but somewhat with different final guest concentrations (see experimental section). FTIR, Raman and PXRD data confirmed the identity of both series of samples (see **Fig. SI-18-20**). The SCO behaviors of **1** and **1b** appear comparable (see **Fig. SI-17**). On the other hand, the magnetic study of **2b** and **3b** revealed an increased residual HS fraction in the low temperature plateau (60 % for **2b** and 50 % for **3b**, see **Fig. SI-17**), albeit the shape of the SCO curves and the transition temperatures remain comparable with compounds **2** and **3**. On the whole, whereas the concentration of inserted guest molecules has a clear impact on the SCO properties, these experiments show also that this parameter cannot explain alone the differences between the SCO behaviors of compounds **2** and **3**. We can thus conclude that the insertion of *cis*- and *trans*-stilbene into the {Fe(bpac)[$Pt(CN)_4$]} network leads to different thermal SCO and LIESST behaviors, thus providing the scope for light-induced modulation of spin states *via* GD-LISC.

3.4. Attempts for guest photoisomerization

The literature reports several MOFs with incorporated optically active species and their successful switching in the solid state.[33] However, the effective photoconversion in the solid state is not only hampered by steric hindrance and intermolecular interactions, but also by the strong UV absorption of the samples (host and guest comprised), which considerably reduces the light penetration depth (~μm) in the relevant UV wavelength range (ca. 260 - 360 nm). This results in very low apparent photoconversion yields in bulk

samples (if the excited volume is too small relative to the analyzed one), and the light irradiation effects on the SCO properties are thus minor. In particular, our efforts to detect photoisomerization and associated magnetic property or structural changes on single crystal, powder or diluted powder samples were unsuccessful (see **Fig. SI-21**). In this context, UV Raman spectroscopy appears as a very relevant combined excitation/detection method. Not only does the focused laser beam provide high UV irradiance, but it also probes *exclusively* the photoexcited sample volume. In addition, *a priori*, both the photoisomerization and SCO processes can be probed concomitantly. We thus acquired variable-temperature Raman spectra with the UV excitation wavelength 355 nm for samples **1-3** between 113 and 293 K (see **Fig. SI-22**). Spectra of the free guest molecules were also acquired as references and control Raman experiments under 532 and 785 nm light excitation were performed. (N.B. At these wavelengths no photoisomerization is expected.)

The UV Raman spectra of each sample present primarily resonance-enhanced modes of the guest molecules, whereas Raman peaks of the host framework are unfortunately hardly discernable. Based on literature data,[28,34] in the *trans*-azobenzene sample (and therefore in compound **1** as well), the *trans*-*cis* isomerization should result in a marked shift of the intense N=N stretching vibration from 1440 cm^{-1} (1433 cm^{-1} in compound **1**) to 1512 cm^{-1}, which was not observed in our room-temperature UV Raman spectra. However, at lower temperatures, we observed the emergence of weak Raman peaks at 1506 cm^{-1} and 1135 cm^{-1} in compound **1**, which could be ascribed to N=N and C-N stretches, respectively, of the *cis* conformer (see **Fig. SI-23**). Indeed, the metastable *cis* species is stabilized at low temperatures, where potential laser-induced heating effects on the sample are balanced.

In the case of the stilbene clathrates **2** and **3**, the low temperature Raman spectra did not reveal any additional feature (see **Fig. SI-22**). Hence we restrict our discussion to the room temperature spectra, which are shown in **Fig. 5** along with the spectra of the pure *trans*- and *cis*-stilbene samples acquired at different excitation wavelengths (see also **Tab. SI-6** and **SI-25**). It is important to note that, in the case of stilbene, isomerization from *trans* to *cis* and *vice versa* can be achieved in solution by UV light, which we confirmed by spectrophotometric measurements (see **Fig. SI-24**). We must mention that the neat *trans*-stilbene sample is strongly fluorescent under 355 nm excitation, which prevents the UV Raman signature of this conformer to be discerned. However, the luminescence of *trans*-stilbene molecules is effectively quenched when they are inserted into the {Fe(bpac)[$Pt(CN)_4$]} matrix. We shall also note here that recent studies have shown that stilbene derivatives may undergo cyclization under UV light leading to the formation of 4a,4b-dihydrophenantrene and subsequent transformation to oxidized and more stable phenanthrene. However, our Raman spectra are not compatible with the formation of the cyclic product.[35] In our experimental conditions, the most important spectral marker is the Raman peak around 965 cm^{-1}, which is present only in the *cis* form due to spectral selection rules.[31] Remarkably, under UV light excitation, neither compound **2** nor **3** display this Raman peak. Whereas solely this result does not consist of an irrefutable proof, it strongly indicates a sizeable *cis* to *trans* photoisomerization in

compound **3**. Unfortunately, the very weak intensity of the Raman signal from the host framework in the 355 nm Raman spectra of compound **3** did not allow us to probe the change of the SCO behavior of the host, which must accompany the *cis* to *trans* photoisomerization of the guest molecules at low temperatures.

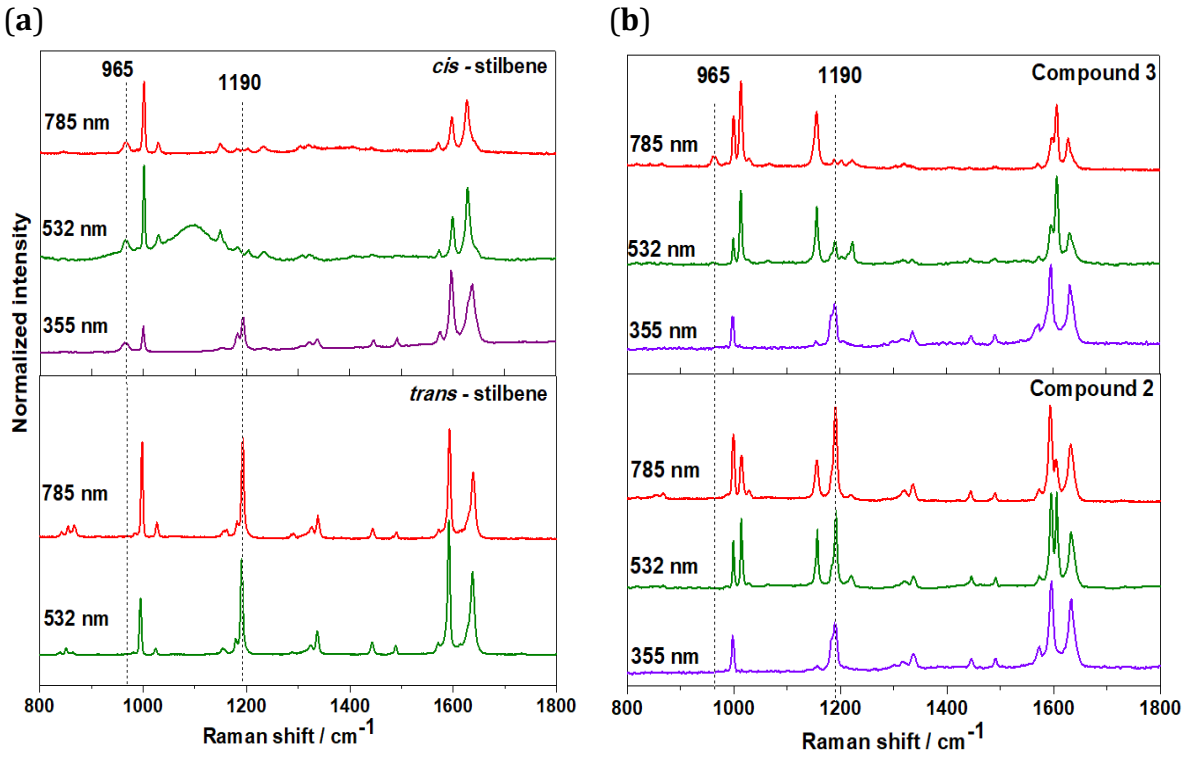

Figure 5. Room-temperature Raman spectra of (**a**) *trans*- (bottom) and *cis*-stilbene (top) obtained using different laser sources and (**b**) compound **2** (bottom) and compound **3** (top).

4. CONCLUSION

In this paper, we have investigated the mutual influence of photoisomerizable guest molecules and a host SCO-MOF framework on the switching properties of both the host and the guest. Single-crystal X-ray analysis, FTIR, Raman spectra and QM/MM simulation provided clear evidence for the successful insertion of *trans*-azobenzene, *trans*-stilbene and *cis*-stilbene molecules into {Fe(bpac)[Pt(CN)$_4$]} frameworks. The magnetic and photomagnetic properties of the host framework were substantially modified through specific interactions with the different guest molecules. The drastic downshift of the spin transition temperatures in the presence of these guest molecules indicates that the SCO properties are altered *via* steric hindrance due to the bulky guest molecules. On the other hand, the different photoisomerization experiments were largely fruitless. Most likely, the steric hindrance and/or specific interactions with the host constitute an unsurmountable barrier for the photoconversion of the guest molecules within the host framework. Nevertheless, UV Raman experiments suggest that guest *cis*-stilbene molecules might be photoisomerized to some extent even inside the pores. This observation calls for further

investigations, which should be extended for different host and guest systems (larger size of pores, guest activation by visible light or temperature), preferably in the form of thin films, in conjunction with adapted excitation/detection methods, such as multiple-wavelength Raman spectroscopy.

Conflict of interest

To the best of our knowledge, there are no conflicts to declare

Acknowledgements. Slovak grant agencies are acknowledged for the financial support (APVV-18-0197, APVV-18-0016, APVV-19-0087, VEGA 1/0125/18, KEGA 018-STU-4). This article was written thanks to the generous support under the Operational Program Integrated Infrastructure for the project: "Strategic research in the field of SMART monitoring, treatment and preventive protection against coronavirus (SARS-CoV-2) ", Project no. 313011ASS8, co-financed by the European Regional Development Fund. BB acknowledges The National Scholarship Programme of the Slovak Republic for the Support of Mobility of Students, PhD Students, University Teachers and Researchers; Tatra Bank Scholarship. IŠ acknowledges financial support from institutional sources of the Department of Inorganic Chemistry, Palacký University Olomouc, Czech Republic and from the Ministry of Education, Youth and Sports of the Czech Republic under the project CEITEC 2020 (LQ1601). The authors thank the platform SIV (Spectroscopie et Imagerie Vibrationnelle) at the University of Bordeaux, funded by the European Union (FEDER) and the Nouvelle Aquitaine region, for access to near-IR and UV Raman spectrometers. JP is grateful to the HPC centre at the Slovak University of Technology in Bratislava, which is a part of the Slovak Infrastructure of High Performance Computing (SIVVP project, ITMS code 26230120002, funded by the European region development funds, ERDF) and to Dr. Christoph Riplinger for enabling the calculation of Raman spectra within the development version of the ORCA software. The authors thank to Xavier Thompson for the participation on the synthesis of reported compounds.

References

1. a) P. Gütlich and H. A. Goodwin, *Spin Crossover in Transition Metal Compounds* I-III, Springer Berlin Heidelberg, Berlin, 2004; b) M. A. Halcrow, *Spin-Crossover Materials: Properties and Applications*, John Wiley & Sons, Chichester, 2013; c) A. Bousseksou, G. Molnár, L. Salmon and W. Nicolazzi, *Chem. Soc. Rev*., 2011, **40**, 3313; c) W. Nicolazzi and A. Bousseksou, *C. R. Chimie*, 2018, **21**, 1060.
2. a) O. Kahn, J. Kröber and C. Jay, *Adv. Mater. 4*., 1992, **11***,* 718; b) J.-F. Létard, P. Guionneau and L. Goux-Capes, in *Spin Crossover in Transition Metal Compounds III*, ed. P. Gütlich and H. A. Goodwin, Springer Berlin Heidelberg, Berlin, 2004, pp. 221–249; c) Y. Garcia, V. Ksenofontov and P. Gütlich, *Hyperfine Interact*., 2002, **139***,* 543; d) G. Molnár, S. Rat, L. Salmon, W. Nicolazzi and A. Bousseksou, *Adv. Mater.,* 2018, **30**, 17003862; e) K. Senthil Kumar and M. Ruben, *Coord. Chem. Rev.*, 2017, **346**, 176.

3. a) J. J. McGarvey and I. Lawthers, *J. Chem. Soc. Chem. Commun.*, 1982, 906; b) I. Lawthers and J. J. McGarvey, *J. Am. Chem. Soc.,* 1984, **106**, 4280; c) J. J. McGarvey, H. Toftlund, A. H. R. Al-Obaidi, K. P. Taylor and S. E. J. Bell, *Inorg. Chem.,* 1993, **32**, 2469.
4. a) S. Decurtins, P. Gütlich, C.P. Köhler, H. Spiering and A. Hauser, *Chem. Phys. Lett.,* 1984, **105**, 1; b) A. Hauser, in *Spin Crossover in Transition Metal Compounds II. Topics in Current Chemistry*, ed. P. Gütlich and H. A. Goodwin, Springer Berlin Heidelberg, Berlin, 2004, pp. 155-198; c) G. Chastanet, M. Lorenc, R. Bertoni and C. Desplanches, *C. R. Chim.*, 2018, **21**, 1075; d) S. Hayami, Z.-Z. Gu, M. Shiro, Y. Einaga, A. Fujishima and O. Sato, *J. Am. Chem. Soc.*, 2000, **122**, 7126; e) I. Šalitroš and J. Pavlik, in *Encyclopedia of Physical Organic Chemistry: Light-Induced Excited Spin State Trapping*, ed. Z. Wang, U. Wille and E. Juaristi, John Wiley & Sons, Hoboken, 2017, pp. 3083-3180.
5. a) M.-L. Boillot, J. Zarembowitch and A. Sour, in *Spin Crossover in Transition Metal Compounds II*, ed. P. Gütlich and H. A. Goodwin, Springer Berlin Heidelberg, Berlin, 2004, pp. 261–276; b) C. Roux, J. Zarembowitch, B. Gallois, T. Granier and R. Claude, *Inorg. Chem.*, 1994, **33**, 2273; c) J. Y. Lallemand, M. L. Boillot, J. Zarembowitch, J. Prunet and S. Chantraine, *New J. Chem.,* 2002, **23**, 179; d) M. M. Khusniyarov, *Chem. Eur. J.*, 2016, **22,** 15178.
6. a) Y. Hasegawa, K. Takahashi, S. Kume and H. Nishihara, *Chem. Commun.*, 2011, **47**, 6846; b) K. Takahashi, Y. Hasegawa, R. Sakamoto, M. Nishikawa, S. Kume, E. Nishibori and H. Nishihara, *Inorg. Chem.*, 2012, **51**, 5188; c) A. Tissot, M. L. Boillot, S. Pillet, E. Codjovi, K. Boukheddaden and L. M. Lawson Daku, *J. Phys. Chem. C,* 2010, **114**, 21715; d) B. Rösner, M. Milek, A. Witt, B. Gobaut, P. Torelli, R. H. Fink and M. M. Khusniyarov, *Angew. Chem. Int. Ed.,* 2015, **54**, 12976; e) L. Poggini, M. Milek, G. Londi, A. Naim, G. Poneti, L. Squillantini, A. Magnani, F. Totti, P. Rosa, M. M. Khusniyarov and M. Mannini, *Mater. Horizons,* 2018, **5**, 506; f) B. Brachňaková and I. Šalitroš, *Chem. Pap.*, 2018, **72**, 773.
7. V. Niel, J. M. Martinez-Agudo, M. C. Muñoz, A. B. Gaspar and J. A. Real, *Inorg. Chem.*, 2001, **40**, 3838.
8. a) Y. Garcia, V. Niel, M. C. Munoz and J. A. Real, in *Spin Crossover in Transition Metal Compounds I*, ed. P. Gütlich and H. A. Goodwin, Springer Berlin Heidelberg, Berlin, 2004, pp. 229–257; b) M. C. Muñoz and J. A. Real, *Coord. Chem. Rev.*, 2011, **255**, 2068; c) P. Gütlich, A. B. Gaspar and Y. Garcia, *Beilstein J. Org. Chem.*, 2013, **9,** 342; d) Z. P. Ni, J. L. Liu, M. N. Hoque, W. Liu, J. Y. Li, Y. C. Chen and M. L. Tong, *Coord. Chem. Rev.*, 2017, **335**, 28; e) C. Bartual-Murgui, N. A. Ortega-Villar, H. J. Shepherd, M. Carmen Muñoz, L. Salmon, G. Molnár, A. Bousseksou and J. A. Real, *J. Mater. Chem.*, 2011, **21**, 7217.
9. M. Ohba, K. Yoneda, G. Agustí, M. C. Muñoz, A. B. Gaspar, J. A. Real, M. Yamasaki, H. Ando, Y. Nakao, S. Sakaki and S. Kitagawa, *Angew. Chem. Int. Ed. Engl.*, 2009, **48**, 4767.
10. a) F. J. Muñoz Lara, A. B. Gaspar, D. Aravena, E. Ruiz, M. C. Muñoz, M. Ohba, R. Ohtani, S. Kitagawa and J. A. Real, *Chem. Commun.*, 2012, **48**, 4686; b) G. Agustí, R.

Ohtani, K. Yoneda, A. B. Gaspar, M. Ohba, J. F. Sánchez-Royo, M. C. Muñoz, S. Kitagawa and J. A. Real, *Angew. Chem. Int. Ed. Engl.*, 2009, **48,** 8944.

11. P. D. Southon, L. Liu, E. A. Fellows, D. J. Price, G. J. Halder, K. W. Chapman, B. Moubaraki, K. S. Murray, J.-F. Létard and C. J. Kepert, *J. Am. Chem. Soc.*, 2009, **131**, 10998.
12. a) X. Bao, H. J. Shepherd, L. Salmon, G. Molnár, M.-L. Tong and A. Bousseksou, *Angew. Chem. Int. Ed. Engl.*, 2013, **52**, 1198; ; b) C. Bartual-Murgui, A. Akou, Ch. Thibault, G. Molnar, Ch. Vieu, L. Salmon and A. Bousseksou, *J. Mat. Chem. C*, 2015, **3**, 1277; c) C. Bartual-Murgui, A. Akou, H. J. Shepherd, G. Molnár, J. A. Real, L. Salmon and A. Bousseksou, *Chem. Eur. J*, 2013, **19**, 15036.
13. a) J. Park, D. Yuan, K. T. Pham, J.-R. Li, A. Yakovenko and H.-C. Zhou, *J. Am. Chem. Soc.*, 2012, **134**, 99; b) J. W. Brown, B. L. Henderson, M. D. Kiesz, A. C. Whalley, W. Morris, S. Grunder, H. Deng, H. Furukawa, J. I. Zink, J. Fraser Stoddart and O. M. Yaghi, *Chem. Sci.*, 2013, **4**, 2858; c) N. Yanai, T. Uemura, M. Inoue, R. Matsuda, T. Fukushima, M. Tsujimoto, S. Isoda and S. Kitagawa, *J. Am. Chem. Soc.*, 2012, **134**, 4501; d) A. Modrow, D. Zargarani, R. Herges and N. Stock, *Dalton Trans.*, 2011, **40**, 4217.
14. a) S. Garg, H. Schwartz, M. Kozlowska, A. B. Kanj, K. Müller, W. Wenzel, U. Ruschewitz and L. Heinke, *Angew. Chem. Int. Ed Engl.*, 2019, **58**, 1193; b) G. H. Clever, S. Tashiro and M. Shionoya, *J. Am. Chem. Soc.*, 2010, **132**, 9973; c) D. Samanta, J. Gemen, Z. Chu, Y. Diskin-Posner, L. J. W. Shimon and R. Klajn, *Proc. Natl. Acad. Sci. U. S. A.*, 2018, **115**, 9379; d) H. Dube, D. Ajami and J. Rebek Jr, *Angew. Chem. Int. Ed Engl.*, 2010, **49**, 3192; e) T. Kusukawa and M. Fujita, *J. Am. Chem. Soc.*, 1999, **121**, 1397.
15. C. Bartual-Murgui, L. Salmon, A. Akou, N. A. Ortega-Villar, H. J. Shepherd, M. C. Muñoz, G. Molnár, J. A. Real and A. Bousseksou, *Chem. Eur. J*, 2012, **18**, 507.
16. a) G. M. Sheldrick, *Acta Crystallogr. Sect. A*, 2015, **A71**, 3; b) G. M. Sheldrick, *Acta Crystallogr. Sect. C*, 2015, **C71**, 3; c) O. Dolomanov, L. J. Bourhis, R. J. Gildea, J. A. K. Howard and H. Puschmann, *J. Appl. Crystallogr.*, 2009, **42**, 339; d) C. F. MacRae, I. Sovago, S. J. Cottrell, P. T. A. Galek, P. mcCabe, E. Pidcock, M. Platings, G. P. Shields, J. S. Stevens, M. Towler and P. A. Wood, *J. Appl. Crystallogr.*, 2020, **53**, 226.
17. a) F. Neese, *WIREs Comput Mol Sci*, 2018, **8**, 33; b) F. Neese, *WIREs Comput Mol Sci*, 2012, **2**, 73; c) S. Grimme, J. G. Brandenburg, C. Bannwarth and A. Hansen, *J. Chem. Phys.* 2015, **143**, 054107; d) C. M. Breneman and K. B. Wiberg, *J. Comput. Chem.*, 1990, **11**, 361; e) J. P. Perdew, K. Burke, and M. Ernzerhof, *Phys. Rev. Lett.*, 1996, **77**, 3865; f) F. Weigend and R. Ahlrichs, *Phys. Chem. Chem. Phys.*, 2005, **7**, 3297; g) D. Andrae, U. Häußermann, M. Dolg, H. Stoll and H. Preuß, *Theor. Chim. Acta*, 1990, **77**, 123; g) F. Neese, *J. Comput. Chem.*, 2003, **24**, 1740; i) J. P. Perdew, M. Ernzerhof and K. Burke, *J. Chem. Phys.*, 1996, **105**, 9982.
18. J.-F. Létard, *J. Mater. Chem.*, 2006, **16**, 2550.
19. a) M. Irie, *Chem. Rev.*, 2000, **100**, 1685; b) D. Gindre, A. Boeglin, A. Fort, L. Mager and K. D. Dorkenoo, *Opt. Express*, 2006, **14**, 9896.
20. K. G. Yager and C. J. Barrett, *J. Photochem. Photobiol. A Chem.*, 2006, **182**, 250.

21. a) H. Rau, in *Photochromism, Molecules and Systems: Azo compounds*, ed. H. Dürr and H. Bouas-Laurent, Elsevier, Amsterdam, 2003, pp. 165–192; b) H. M. D. Bandara and S. C. Burdette, *Chem. Soc. Rev.*, 2012, **41**, 1809.
22. G. Molnár, V. Niel, A. B. Gaspar, J.-A. Real, A. Zwick, A. Bousseksou and J. J. McGarvey, *J. Phys. Chem. B*, 2002, **106**, 9701.
23. a) P. Hamm, S. M. Ohline and W. Zinth, *J. Chem. Phys.*, 1997, **106**, 519; b) L. Duarte, R. Fausto and I. Reva, *Phys. Chem. Chem. Phys.*, 2014, **16**, 16919.
24. a) V. Stepanić, G. Baranović and V. Smrečki, *J. Mol. Struct.*, 2001, **569**, 89; b) Z. Zhuang, J. Cheng, X. Wang, Y. Yin, G. Chen, B. Zhao, H. Zhang and G. Zhang, *J. Mol. Struct.*, 2006, **794,** 77.
25. a) C. H. Choi and M. Kertesz, *J. Phys. Chem. A*, 1997, **101**, 3823; b) J. F. Arenas, I. L. Tocón, J. C. Otero and J. I. Marcos, *J. Mol. Struct.*, 1995, **349,** 29.
26. a) Z. Meić, T. Šuste, G. Baranović, V. Smrečki, S. Holly and G. Keresztury, *J. Mol. Struct.*, 1995, **348**, 229; b) C. Pecile and B. Lunelli, *Can. J. Chem.*, 1969, **47**, 243.
27. G. Agusti, S. Cobo, A. B. Gaspar, G. Molnár, N. O. Moussa, P. Á. Szilágyi, V. Pálfi, C. Vieu, M. Carmen Muñoz, J. A. Real and A. Bousseksou, *Chem. Mater.*, 2008, **20**, 6721.
28. C. M. Stuart, R. R. Frontiera and R. A. Mathies, *J. Phys. Chem. A*, 2007, **111**, 12072.
29. H. Watanabe, Y. Okamoto, K. Furuya, A. Sakamoto and M. Tasumi, *J. Phys. Chem. A*, 2002, **106**, 3318.
30. T. Egawa, K. Shinashi, T. Ueda, E. J. Ocola, W.-Y. Chiang and J. Laane, *J. Phys. Chem. A*, 2014, **118**, 1103.
31. K. Furuya, K. Kawato, H. Yokoyama, A. Sakamoto and M. Tasumi, *J. Phys. Chem. A*, 2003, **107**, 8251.
32. A. Akou, C. Bartual-Murgui, K. Abdul-Kader, M. Lopes, G. Molnár, C. Thibault, C. Vieu, L. Salmon and A. Bousseksou, *Dalton Trans.*, 2013, **42**, 16021.
33. a) W. Zhou, S. Grosjean, S. Bräse and L. Heinke, *Z. Phys. Chem.*, 2018, **233**, 15; b) X. Yu, Z. Wang, M. Buchholz, N. Füllgrabe, S. Grosjean, F. Bebensee, S. Bräse, C. Wöll and L. Heinke, *Phys. Chem. Chem. Phys.*, 2015, **17**, 22721; c) K. Müller, J. Helfferich, F. Zhao, R. Verma, A. B. Kanj, V. Meded, D. Bléger, W. Wenzel and L. Heinke, *Adv. Mater.*, 2018, **30***,* 1706551; d) H. Meng, C. Zhao, M. Nie, C. Wang and T. Wang, *ACS Appl. Mater. Interfaces*, 2018*,* **10***,* 32607; e) Z. Wang, S. Grosjean, S. Bräse and L. Heinke, *Chem. Phys. Chem.*, 2015, **16**, 3779.
34. T. Fujino and T. Tahara, *J. Phys. Chem. A*, 2000, **104**, 4203.
35. a) J.-M. Rodier, X. Ci and A. B. Myers, *Chem. Phys. Lett.*, 1991, **183**, 55; b) F. Capitani, M. Höppner, L. Malavasi, C. Marini, P. Dore, L. Boeri and P. Postorino, *J. Phys. Conf. Series*, 2017, **950**, 042017.

Graphical abstract

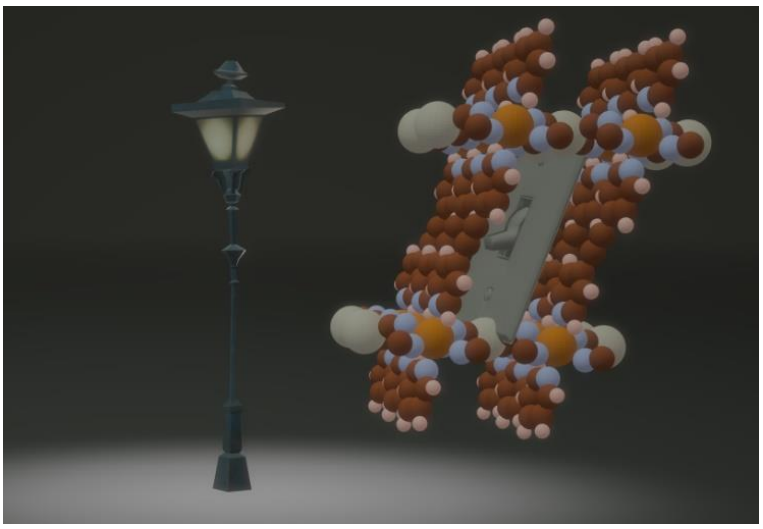

The introduction of photoactive guest molecules into a spin crossover 3D metal organic framework alters the switchable properties of both host and guest.